

Electronic Supplementary Information

Molecular Stacking Dependent Phosphorescence-Fluorescence Dual Emission on Single Luminophore for Self-Recoverable Mechanoconversion of Multicolor Luminescence

Hongwei Wu^{a,b}, Cheng Hang^a, Xin Li^c, Liyuan Yin^a, Mingjie Zhu^a, Jian Zhang^a, Yunyun Zhou^a,

Hans Ågren^c, Qing Zhang^{b*} and Liangliang Zhu^{a*}

^a State Key Laboratory of Molecular Engineering of Polymers,

Department of Macromolecular Science, Fudan University, Shanghai 200433, China.

^b Shanghai Key Lab of Polymer and Electrical Insulation, School of Chemistry and Chemical Engineering, Shanghai Jiaotong University, Shanghai 200240, China

^c Division of Theoretical Chemistry and Biology, School of Biotechnology, KTH Royal Institute of Technology, SE-10691 Stockholm, Sweden

Contents

- Section S1 Materials and synthesis, Page S3-S6
- Section S2 Self-assemblies and preparation for solid films, Page S7
- Section S3 Computational details, Page S8
- Section S4 Emission spectra of **2** and **3**, Page S9
- Section S5 Photoluminescent lifetime of **2** and **3** in solution, Page S10
- Section S6 Absorption, emission and excitation spectra of **1** in solution, Page S11
- Section S7 The photographs, TEM images and chromaticity diagram of **1** in ethanol and THF, Page S12
- Section S8 Emission spectra of **2** and **3** in solid film, Page S13
- Section S9 Simulation structure of molecules **1**, Page S14
- Section S10 Solvent-accessible surface area (SASA) of compound **1** of simulations, Page S15
- Section S11 Number of intermolecular and intramolecular hydrogen bonds, Page S16
- Section S12 TEM images of **2** and **3**, Page S17
- Section S13 Multicolor luminescence in the solid state of **1**, Page S18
- Section S14 FT-IR spectra of films of **1** and the proposed mechanism for the phosphorescence-to-fluorescence radiative transfer, Page S19-20
- Section S15 Emission spectra, chromaticity diagram and XRD for mechanical stimuli, Page S21
- Section S16 NMR, MALDI-TOF MS of compounds, Page S22-27
- Section S17 References, Page S28

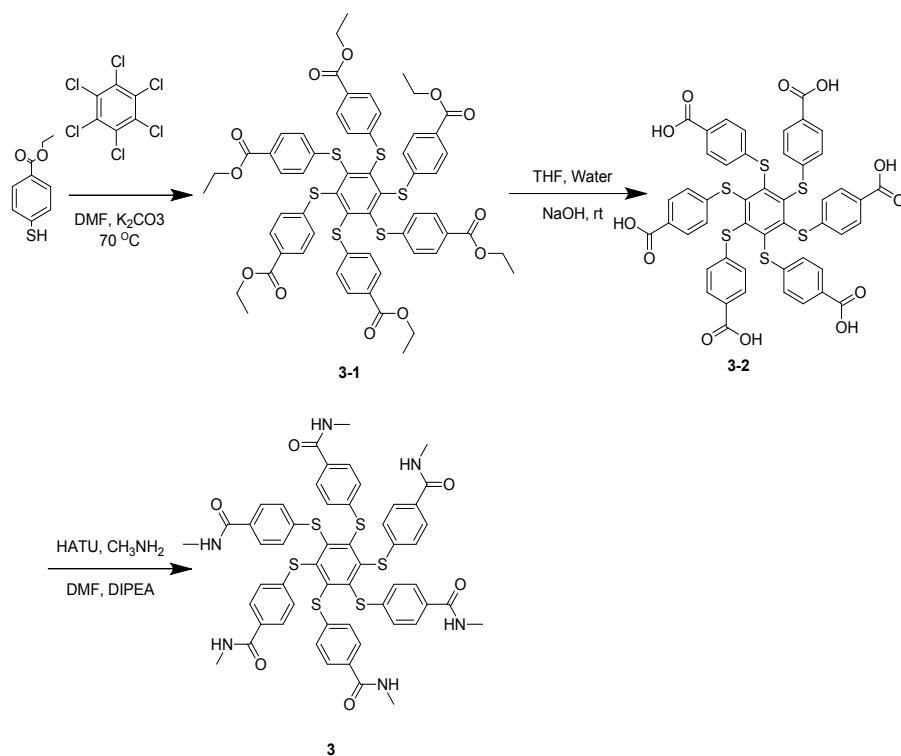


Figure S1. Synthetic route for compound **1**, **2** and **3**.

Synthesis of compound 1-1: This compound was prepared according to a similar procedure described in literature.

S1

Synthesis of compound 1: A dry condenser was installed to an oven-dried, 100 mL two-necked round-bottom flask under nitrogen. **1**, **2**, **3**, **4**, **5**, **6**-Hexafluorobenzene (372 mg, 2 mmol), compound **1-1** (4.08g, 24 mmol) and DMI (20.0 mL) were added successively. Powder NaH (60% purity, 960 mg, 24 mmol) was added. The mixture was cooled in an ice-bath, followed by the formation of a foam and the color of the mixture changed from yellow to orange. At the end of the addition, the reaction mixture was left at $20\text{ }^\circ\text{C}$ for 18 h when stirred with a magnetic bar. A yellow precipitate was generated with addition of a NaOH (1M, 0.25 L) aqueous solution. The solid was collected by filter and washed by water, EA, ethanol, acetone to obtain yellow powder (1 g, 46%). ^1H NMR (400 MHz, $DMSO-d_6$, 298 K): δ =2.03 (s, 18H), 7.14 (d, J = 8.4 Hz, 12H), 7.49 (d, J = 8.4 Hz, 12H), 9.99 (s, 6H). ^{13}C NMR

(100 MHz, DMSO- d_6 , 298 K): δ = 168.80, 138.95, 129.97, 127.76, 120.29, 109.99, 24.46. MS: MALDI-TOF MS, m/z: [M + H]⁺ 1069.4.

Synthesis of compound 2: Compound **1** (267 mg, 0.25 mmol), hydrochloric acid (30 ml) and 1,4-dioxane (30 mL) were refluxed for 18h at a two-necked round-bottom flask under nitrogen, and then the solvent was removed by vacuum distillation while a NaOH (1M, 0.1 L) aqueous solution was added and filtered to collect solid, and it was washed by water, EA, ethanol, acetone to obtain a yellow powder (100 mg, 49%). ¹H NMR (400 MHz, DMSO- d_6 , 298 K): δ = 5.33 (s, 12H), 6.47 (d, J = 8.4 Hz, 12H), 6.97 (d, J = 8.4 Hz, 12H). ¹³C NMR (100 MHz, DMSO- d_6 , 298 K): δ = 149.43, 130.38, 129.30, 117.90, 114.93. MS: MALDI-TOF MS, m/z: [M + H]⁺ 817.19.

Synthesis of compound 3-1: Hexachlorobenzene (2.84 g, 2 mmol, 1.00 eq.), dry K₂CO₃ (2.48 g, 18 mmol, 9 eq.) and ethyl 4-mercaptobenzoate (1.68 g, 18 mmol, 9 eq.) were added into a round bottom flask capped with a septum under an argon atmosphere. Dry DMF (30 mL) was injected via a syringe and the mixture was stirred at 60 °C for 40 h. Water (200 mL) was poured into the flask while stirring, and a yellow precipitate appeared. After collecting the solid by filtration, it was rinsed with ethanol (10 mL), diethyl ether (20 mL), and then dried under high vacuum (1.2 g, 52%). ¹H NMR (400 MHz, CDCl₃, 298 K): δ = 1.42 (t, J = 8.0 Hz, 18H), 4.38 (m, 12H), 6.95 (m, 12H), 7.87 (m, 12H). ¹³C NMR (100 MHz, CDCl₃, 298 K): δ = 14.31, 61.09, 126.98, 128.57, 130.31, 142.55, 147.93, 165.74. MS: MALDI-TOF MS, m/z: [M + H]⁺ 1158.5471.

Synthesis of compound 3-2: Compound **3-1** (1.15g, 10 mmol) was dissolved in THF (30 mL), and an aqueous solution of NaOH (2 M, 5 mL) was poured into the flask while stirring. The reaction mixture was left at 20 °C for 18 h when stirred with a magnetic bar, followed by addition of a HCl (1M, 200 mL) solution. The solid was collected by

filter and washed by water, EA, ethanol, acetone to obtain yellow powder (600 mg), which was used for the next step directly without purification.

Synthesis of compound 3: 3-2 (495 mg, 0.5 mmol, 1 eq) and HATU (2.28g, 6mmol, 12 eq) were dissolved in DMF (10 mL) and stirred for 15min at a two-necked round-bottom flask under nitrogen, and then methylamine (372mg, 6 mmol, 12 eq) and DIPEA (2 ml) were added and the mixture was stirred at room temperature for 18h, followed by addition of water and filtered to collect solid. It was washed by water, EA, ethanol, acetone to obtain a powder compound (300 mg, 56%). ¹H NMR (400 MHz, DMSO-d₆, 298 K): δ = 2.79 (d, J = 4.0 Hz, 18H), 7.09 (d, J = 8.0 Hz, 12H), 7.69 (d, J = 8.0 Hz, 12H), 8.36 (m, 6H). ¹³C NMR (100 MHz, DMSO-d₆, 298 K): δ = 166.38, 147.32, 140.93, 132.47, 128.51, 126.99, 26.75. MS: MALDI-TOF MS, m/z: [M + H]⁺ 1068.52.

Section S2

Self-assemblies in solution: Compound **1-3** (6 mg) were dissolved in DMF (10 mL) and divided into 10 parts (each 1ml), followed by addition into DMF and water to obtain a variety of different proportions. TEM, UV/Vis and PL were used for the analysis of the solutions.

Preparation of solid state film with blue luminescence: Compound **1** (3 mg) was dissolved in DMF (6 mL) and water (4 mL), and then the above solution was dropcasted onto a clean glass substrate. The solvent was removed by placing at 40 °C and in vacuum for 24 h.

Preparation of solid state film with white luminescence: Compound **1** (3 mg) was dissolved in ethanol (10 mL), and then the above solution was dropcasted onto a clean glass substrate. The solvent was removed by placing at 40 °C for 20 min.

Preparation of solid state film with yellow luminescence: Compound **1** (3 mg) was dissolved in THF (10 mL), and then the above solution was dropcasted onto a clean glass substrate. The solvent was removed by placing at 40 °C for 20 min.

Section S3.

Computational details. The geometry of compound **1** was optimized by density functional theory (DFT) calculations using the hybrid B3LYP functional^{S2} and the double-zeta 6-31G(d) basis set^{S3}. The electrostatic potential of the molecules was calculated at the HF/6-31G(d) level of theory, from which partial atomic charges were derived according to the restrained electrostatic potential (RESP)^{S4} procedure. The bonded and nonbonded parameters were adopted from the general Amber force field (GAFF)^{S5}. MD simulations of **1** were conducted in aqueous solutions using the GROMACS program package^{S6}. The starting structure was generated by randomly inserting ten molecules in a cubic box of dimension $10 \times 10 \times 10 \text{ nm}^3$, followed by solvation of around 32000 water molecules and subject to 100-ns MD simulations under ambient temperature and pressure.

Section S4

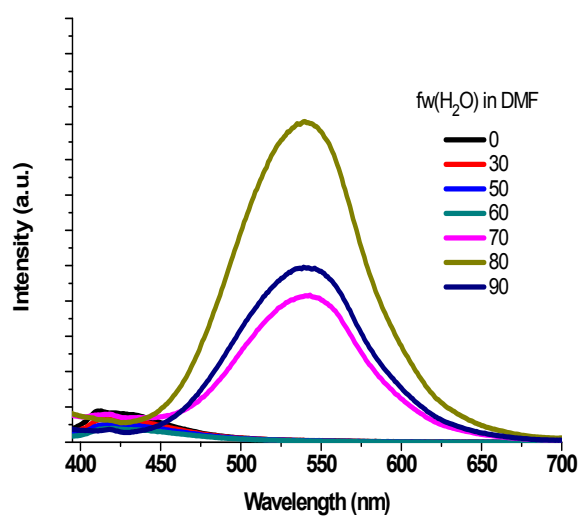


Figure S2. Emission spectra of **2** in DMF/H₂O with a series of water fractions. These measurements were performed at room temperature with the concentration of 60 μ M.

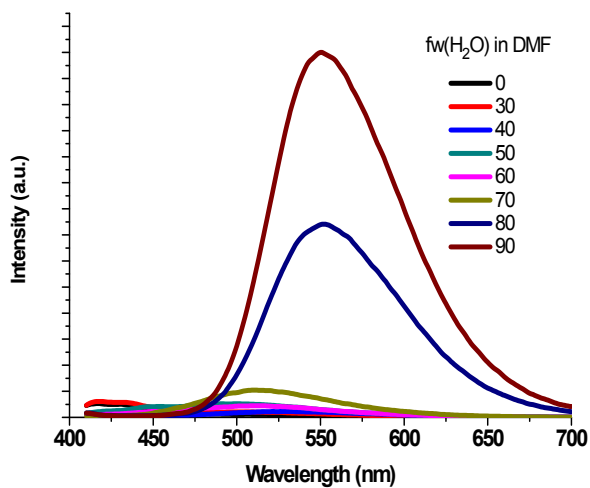


Figure S3. Emission spectra of **3** in DMF/H₂O with a series of water fractions. These measurements were performed at room temperature with the concentration of 60 μ M.

Section S5

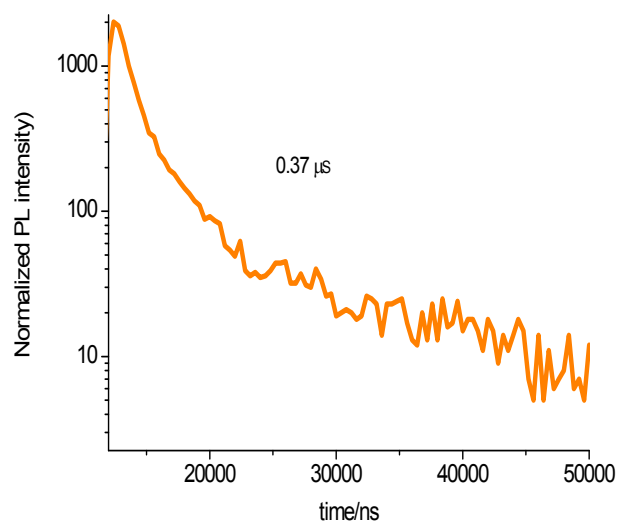


Figure S4. Photoluminescent lifetime of **2** in DMF/H₂O=20:80 measured at 550 nm emission upon excitation at 345 nm.

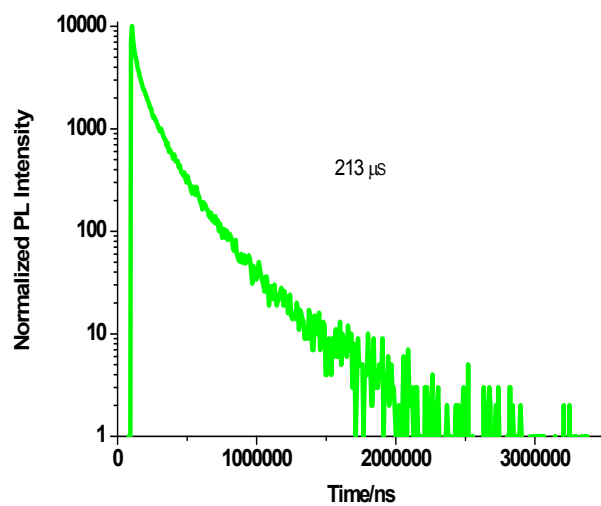


Figure S5. Photoluminescent lifetime of **3** in DMF/H₂O=20:80 measured at 550 nm emission upon excitation at 345 nm.

Section S6

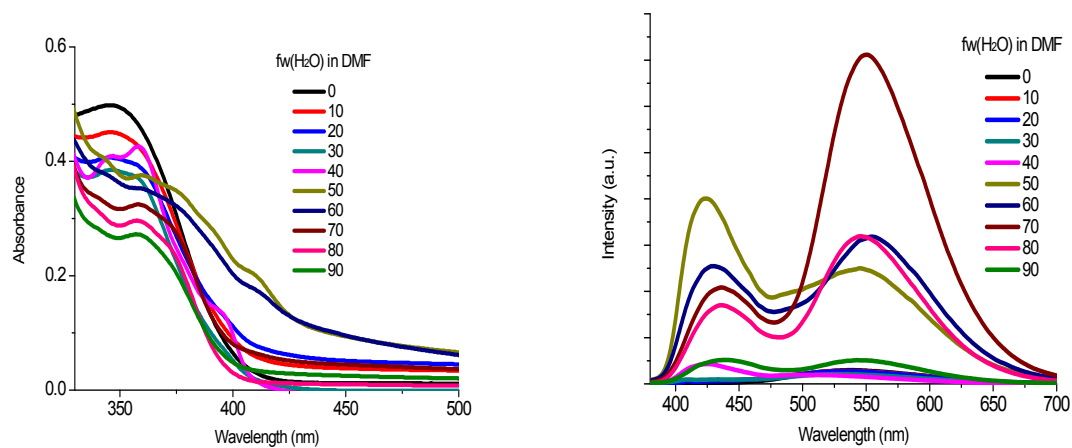


Figure S6. Absorption (left) and emission (right) spectra of **1** (a) in DMF/H₂O with a series of water fractions. All measurements were performed at room temperature with the concentration of 60 μ M.

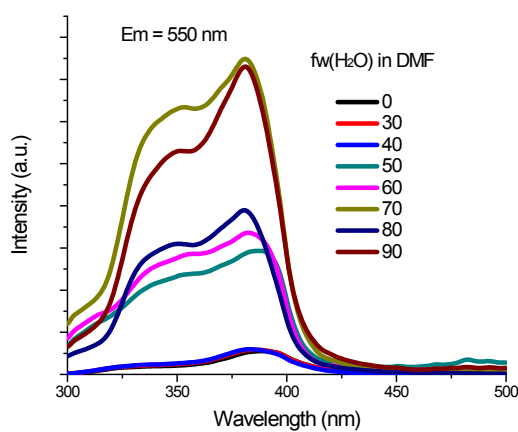


Figure S7. Excitation Spectra of **1** in in DMF/H₂O with a series of water fractions. All measurements were performed at room temperature with the concentration of 60 μ M.

Section S7

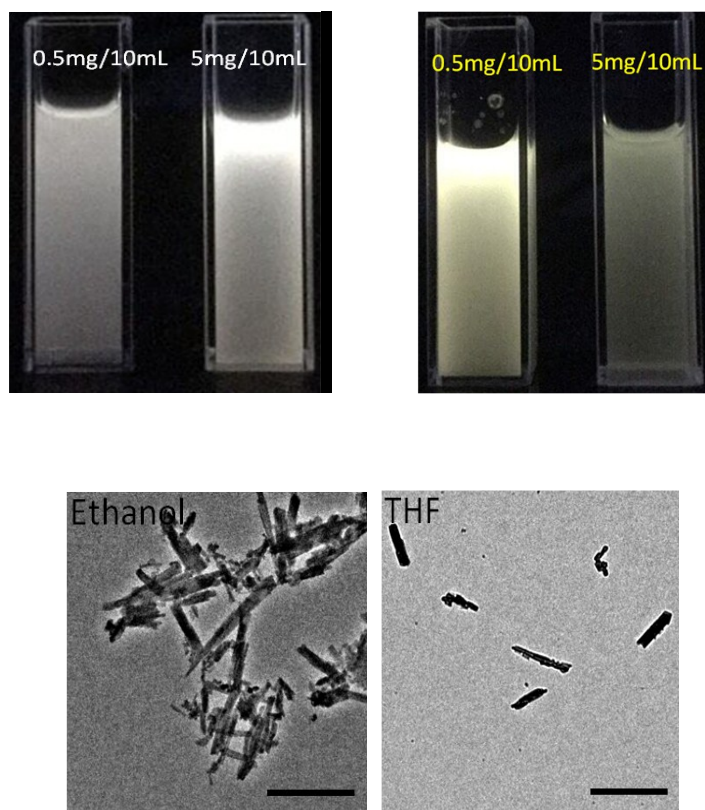


Figure S8. The photographs (under a UV light, 365 nm) and TEM images (Scale bar: 2 μm .) of **1** in ethanol and THF with different concentrations

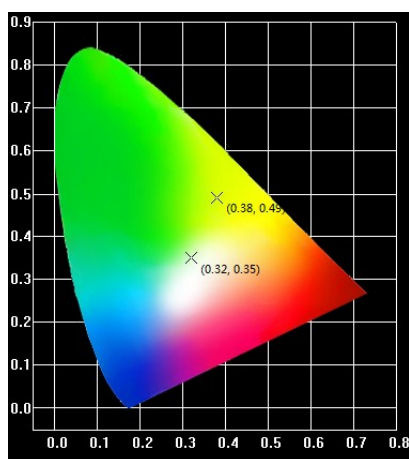


Figure S9. CIE 1931 chromaticity diagram signifying the luminescent color coordinates for **1** in ethanol (0.32, 0.35) and in THF (0.38, 0.49).

Section S8

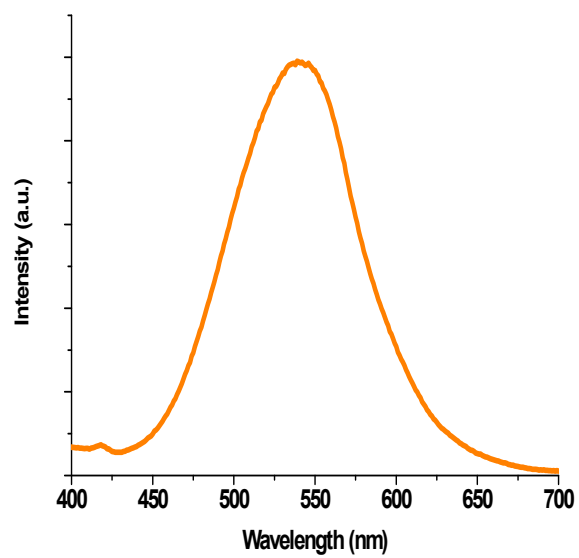


Figure S10. Emission spectra upon 365 nm excitation films of **2**

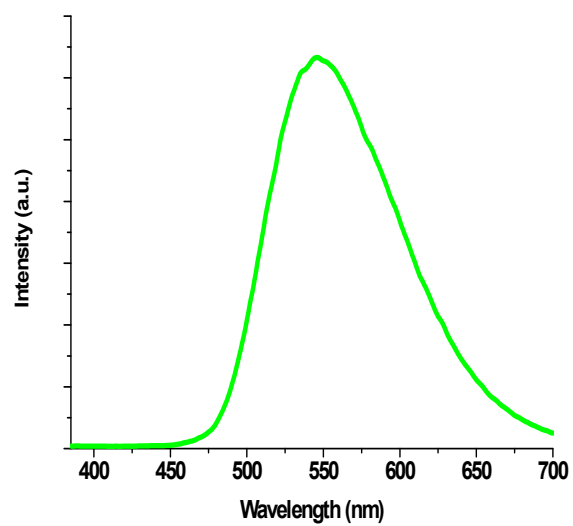


Figure S11. Emission spectra upon 365 nm excitation films of **3**.

Section S9

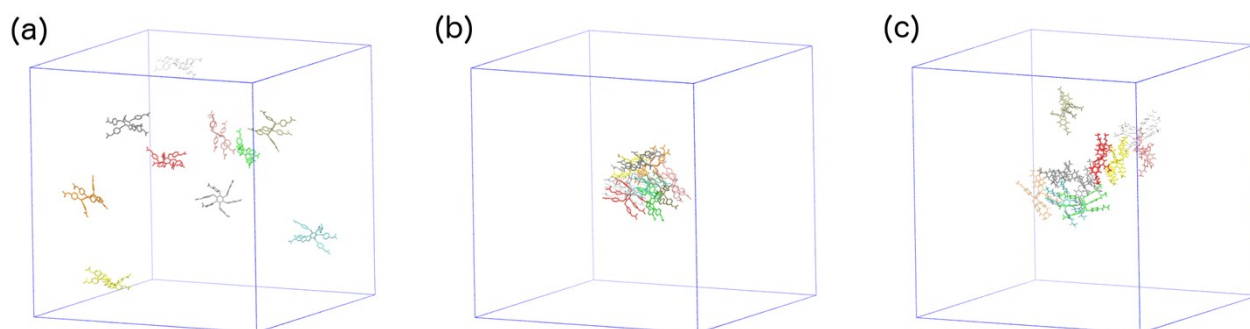


Figure 12. (a) Starting structure of molecules **1**. (b) Final structure of molecules **1** in aqueous solution. (c) Final structure of molecules **1** in mixed DMF/water solution. Solvent molecules are omitted for clarity.

Section S10

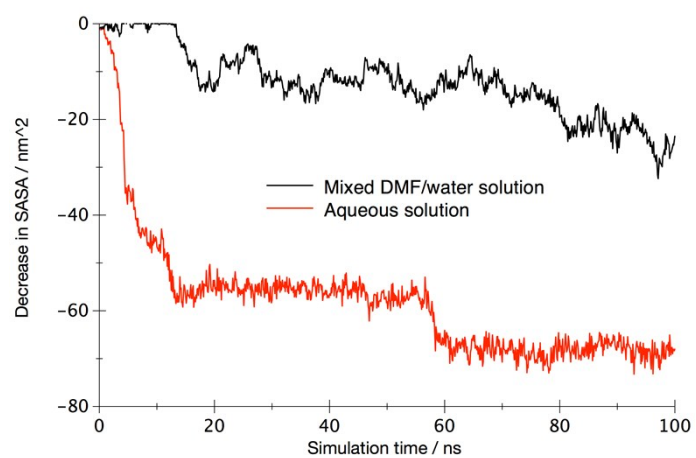


Figure S13. Decrease in solvent-accessible surface area (SASA) of compound **1** during the simulations in aqueous solution and mixed DMF/H₂O solution.

Section S11

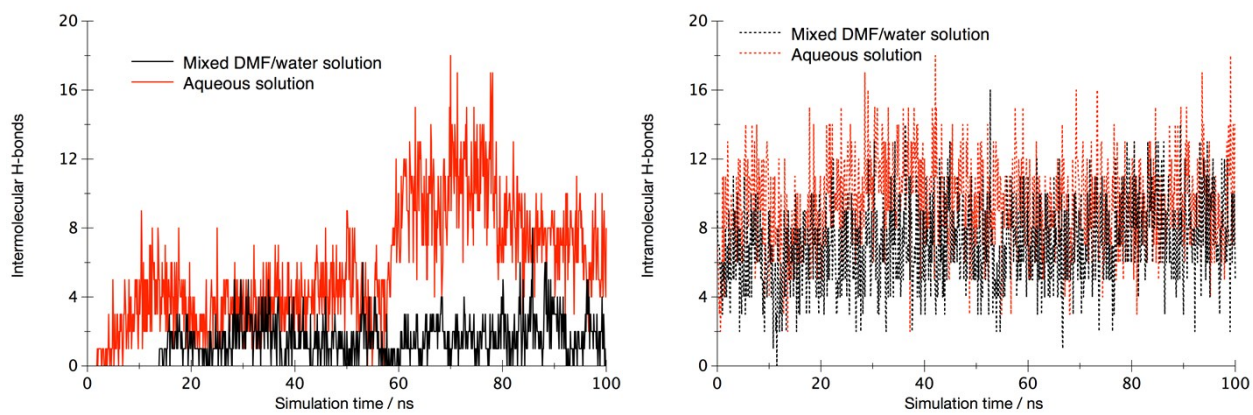


Figure S14. Number of intermolecular and intramolecular hydrogen bonds among **1** in the self-assemblies in aqueous solution and mixed DMF/H₂O solution.

Section S12

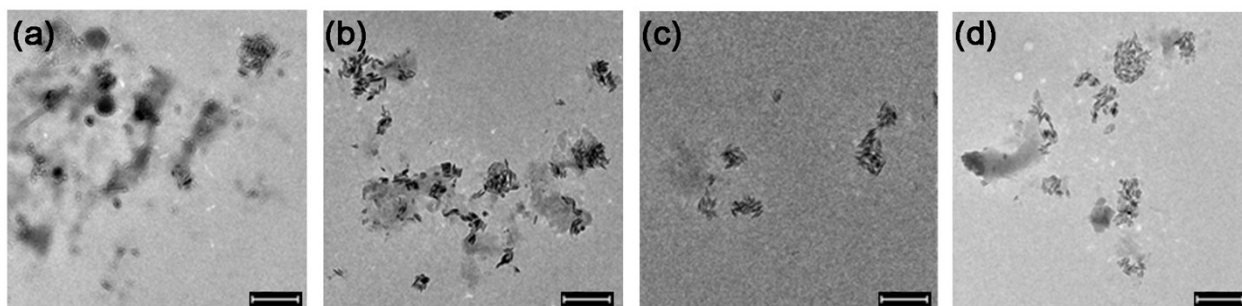


Figure S15. TEM images of **2** prepared from (a) DMF with 30% water, (b) DMF with 60% water, (c) DMF with 70% water and (d) DMF with 80% water. Scale bar: 500 nm.

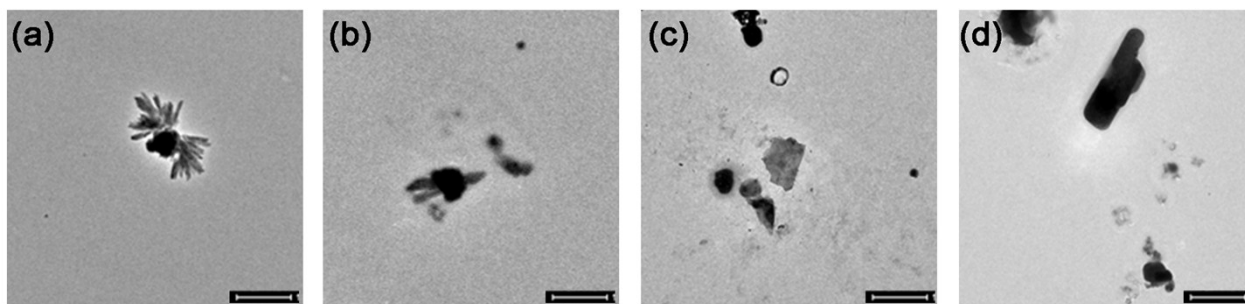


Figure S16. TEM images of **3** prepared from (a) DMF with 40% water, (b) DMF with 50% water, (c) DMF with 60% water and (d) DMF with 70% water. Scale bar: 1 μ m.

Section S13

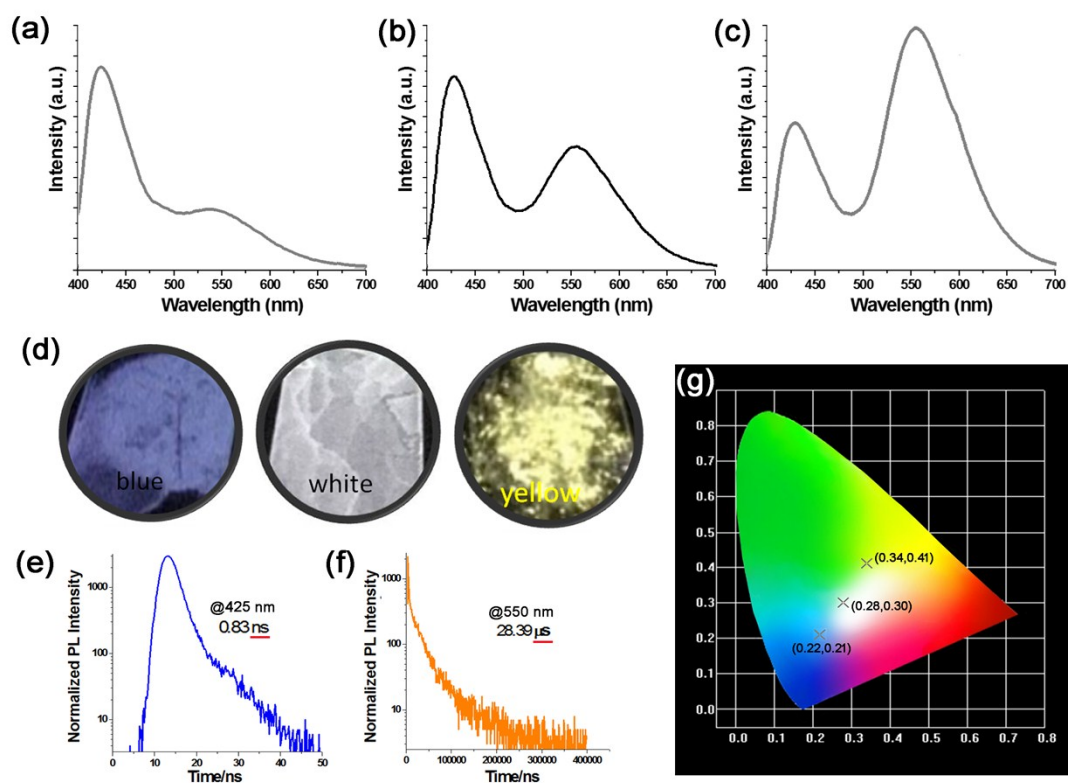


Figure S17. RTP/FL dual-band based multicolor luminescence in the solid state: Emission spectra upon 365 nm excitation films of **1** with a (a) blue, (b) white and (c) yellow luminescence. (d) The photographs of the corresponding films in (a) under a UV light (365 nm). Photoluminescent lifetime of the film of **1** with dual-band measured at (e) 425 nm and (f) 550 nm emission upon excitation at 345 nm. (g) CIE 1931 chromaticity diagram signifying the luminescent color coordinates for the corresponding states in (d). All measurements were performed at room temperature.

Solid-state emissive organic materials are more popular for practical thin-film-device applications. Owing to the AIEE effect of the single luminophore, the solid-state emission properties of **1** can also be explored. With reference to the self-assembly conditions in solution, films with a blue, white and yellow luminescence can be straightforwardly prepared. Figures S17a- S17d show the dual-emission behavior and the multicolor luminescence of the films of **1**. Similar to the case in solution, the dual bands in the solid film are also composed by RTP and FL, after the monitoring of PL lifetime (Figure S17e and S17f). Meanwhile, these films can exhibit an even higher quantum yield ranging from 9.4% to 13.7%. Their luminescent color tones can also be well distinguished by the CIE coordinates (Figure S17g). We emphasize that such a highly emissive multicolor luminescence in the solid state still refers to a single luminophore process without any assistance of matrix materials or templates. Although the films of **2** and **3** can also produce strong emission (see Figure S10 and S11), the dual-emission behavior is still not present.

Section S14

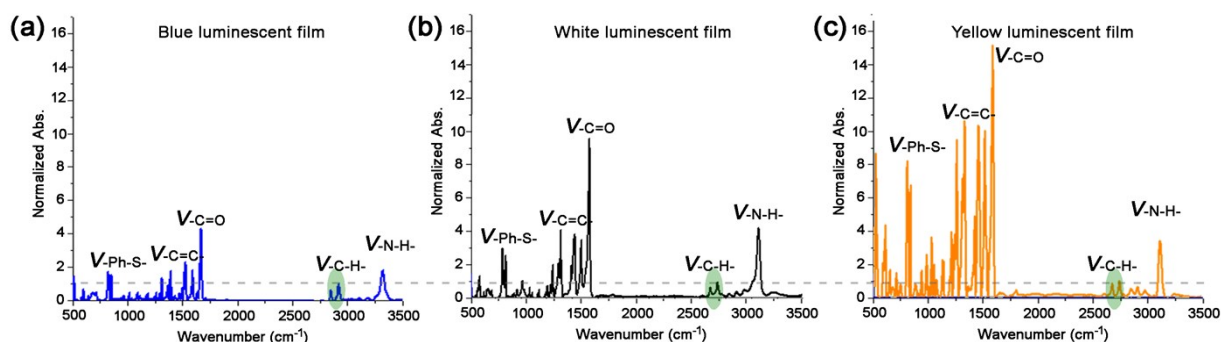


Figure S18. Normalized FT-IR spectra of films of **1** with a (a) blue, (b) white and (c) yellow luminescence.

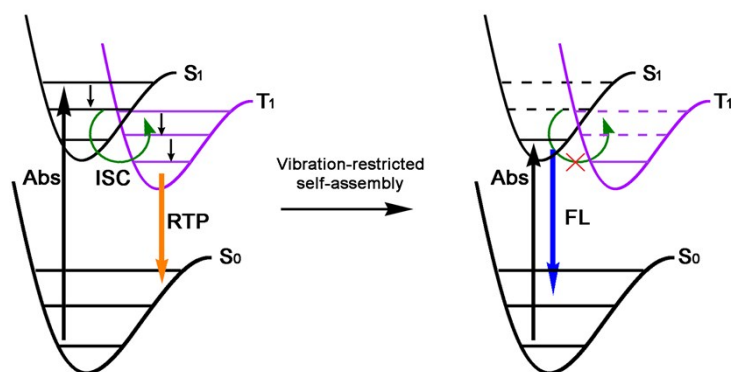


Figure S19. Proposed mechanism for the phosphorescence-to-fluorescence radiative transfer driven by the vibration-restricted self-assembly of **1**.

Having established the chemical structure dependence of the peculiar self-assembling, we turn to investigate the conversion mechanism of the generation of the RTP-FL dual-band emission. Considering that the intersystem crossing for triplet-state radiative decay largely relies on the overlap of the vibrational levels of the excited states, we obtained the molecular vibrational information of the self-assemblies of **1** by FT-IR. Since the methyl group on the asterisk molecule is normally located at the rim of these self-assembly conformations, it would be reasonable that the -C-H- stretching has a minimum sensitivity to the aggregation. Hence, the corresponding peaks around 2919 cm^{-1} ($V_{\text{C-H}}$) was set as the internal standard to compare the normalized FT-IR spectra among the three films. We find that the relative intensity of other vibration signals ($V_{\text{Ph-S}}$, $V_{\text{C=C}}$, $V_{\text{C=O}}$ and $V_{\text{N-H}}$) is close to the internal standard in the blue luminescent film (Figure S18a). However, these peaks became quite strong relative to the internal standard in the white and yellow luminescent films (Figure S18b and S18c). In terms of the above morphological studies, a mechanism for the self-assembly induced radiative transfer from RTP to FL can be

proposed (see Figure S19). Upon the vibration-restricted effect from long nanorods, the electron at S_0 has less chance to be transited to the vibrational levels of S_1 which are overlapping those of T_1 . Hence the ISC process can effectively be inhibited to give birth to FL instead of RTP. For the cases from relatively short nanorods, the molecular vibrations are still active and the electronic state will experience vibrational relaxation, followed by ISC for the RTP radiative decay. In this way, the proportion of RTP-FL dual emission depended on molecular stackings was further confirmed.

Section S15

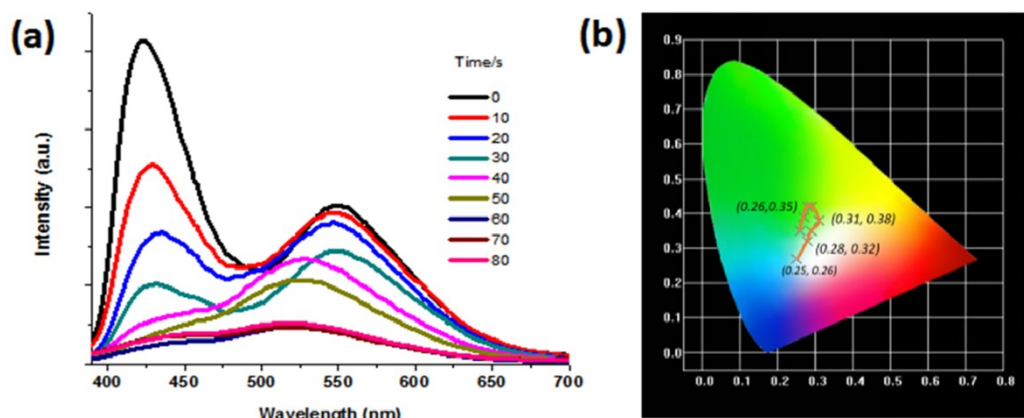


Figure S20. (a) Emission spectra upon 365 nm excitation films of **1** with grinding for different time. (b) CIE 1931 chromaticity diagram signifying the luminescent color coordinates for the corresponding states in (a). All measurements were performed at room temperature.

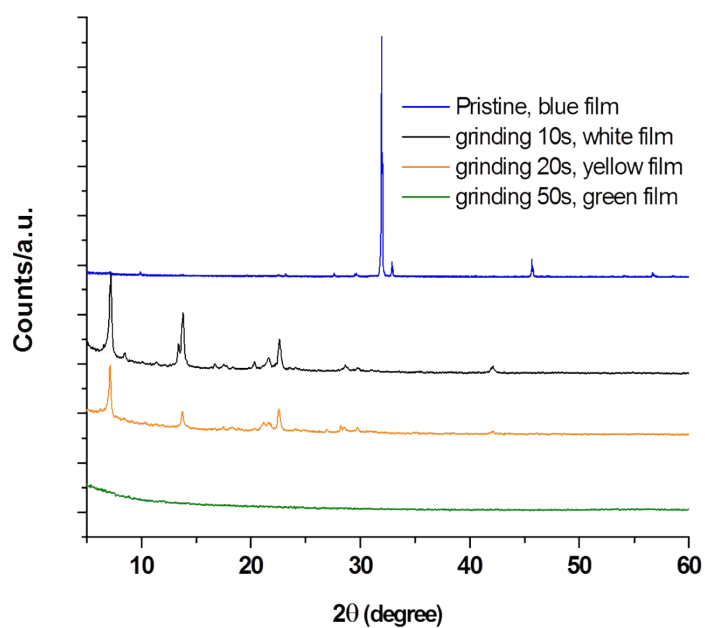
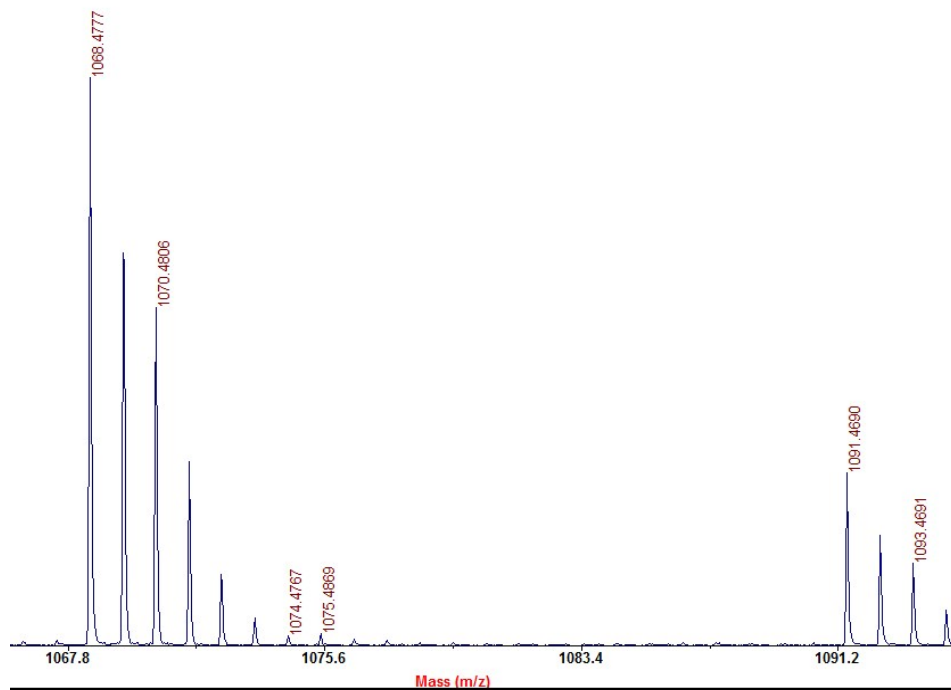
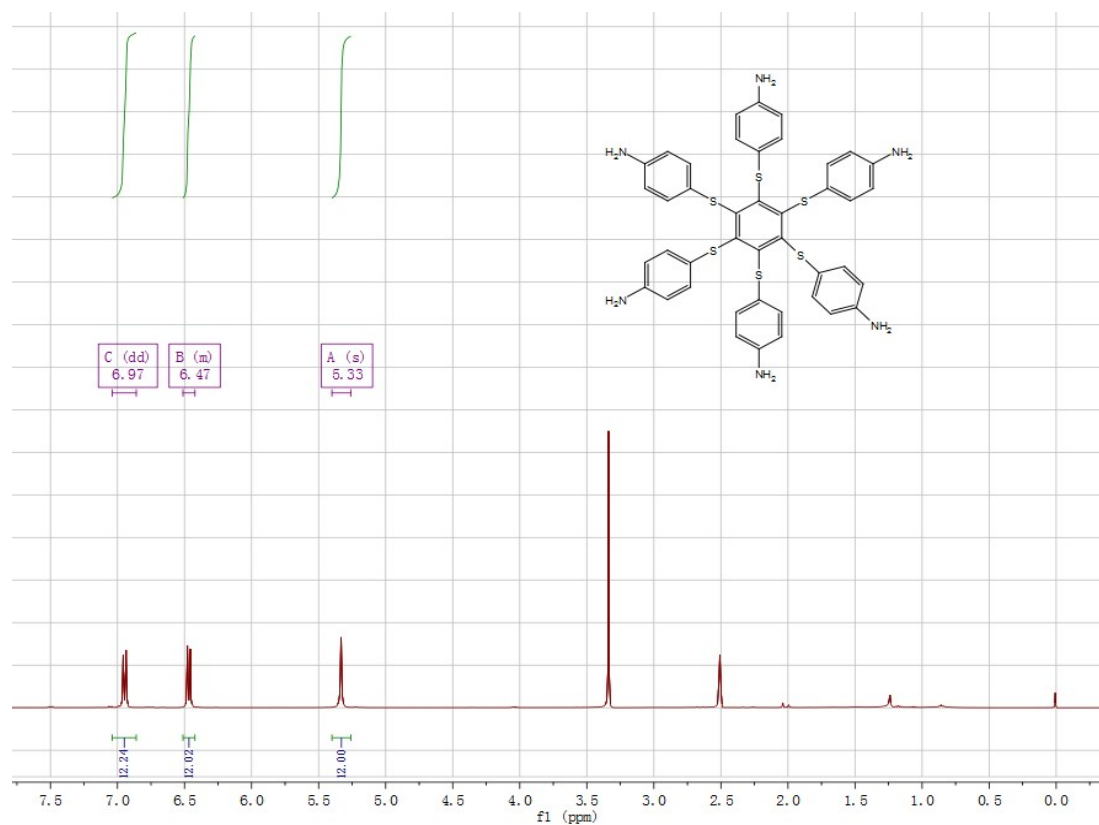


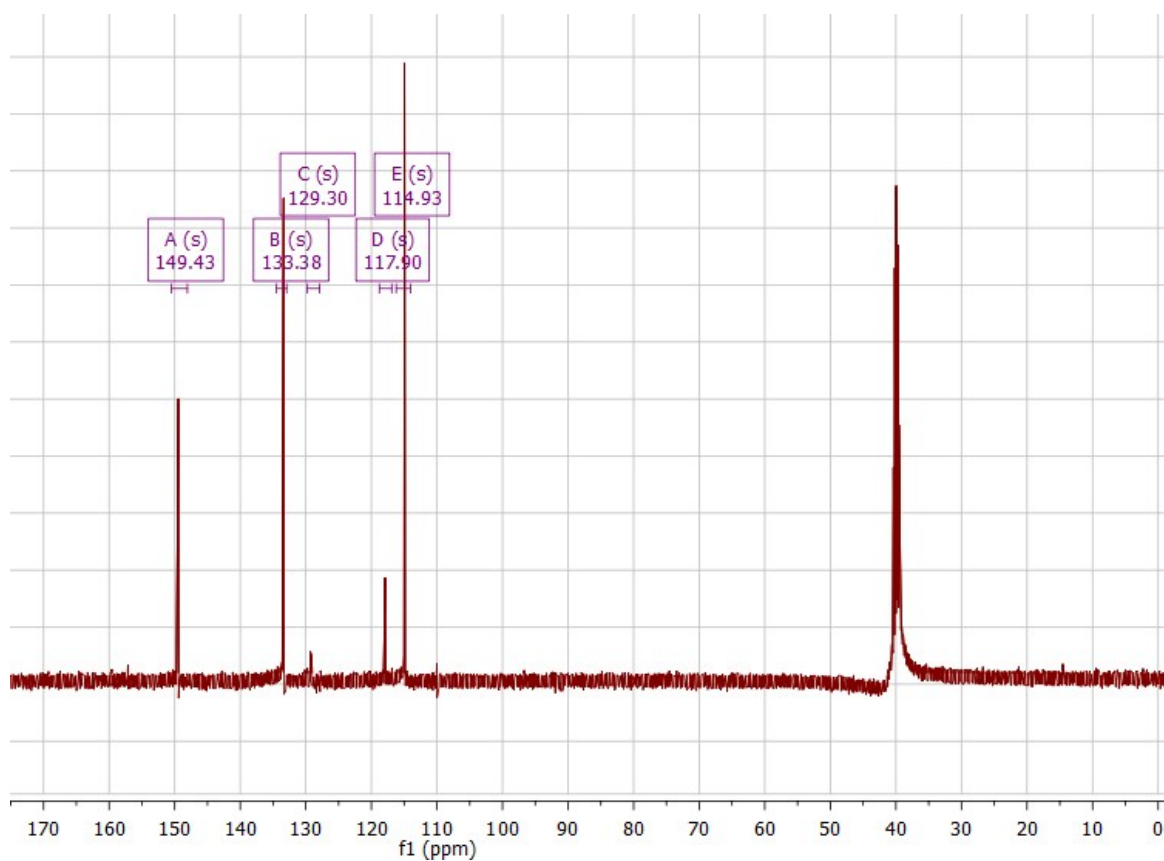
Figure S21. The PXRD of the Pristine and grinded films of **1**.



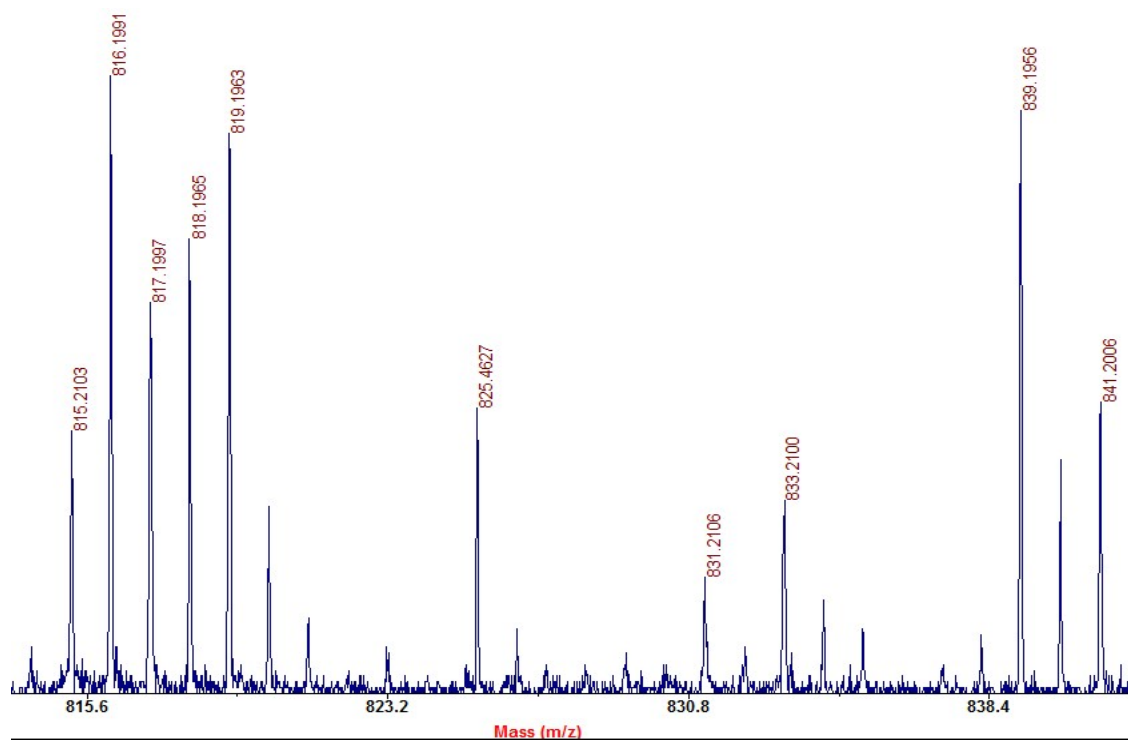
MALDI-TOF MS full spectrum of **1**



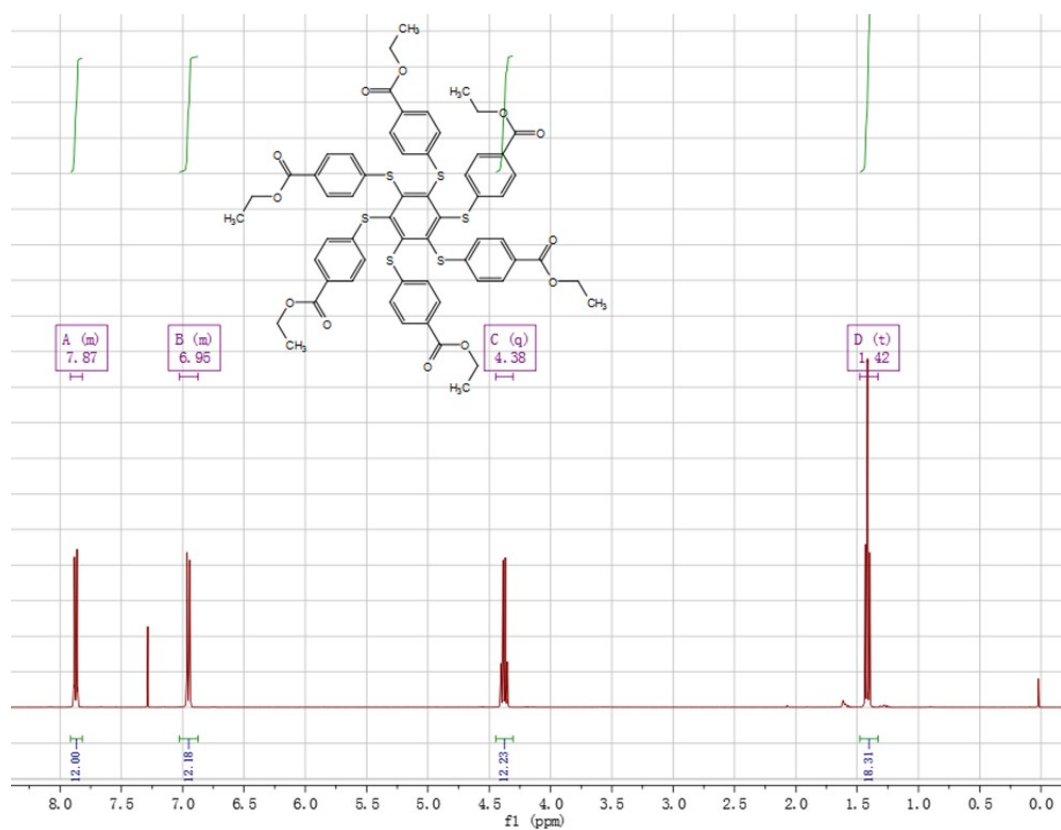
^1H NMR spectra (400 MHz, DMSO-d_8 , 298 K) of **2**



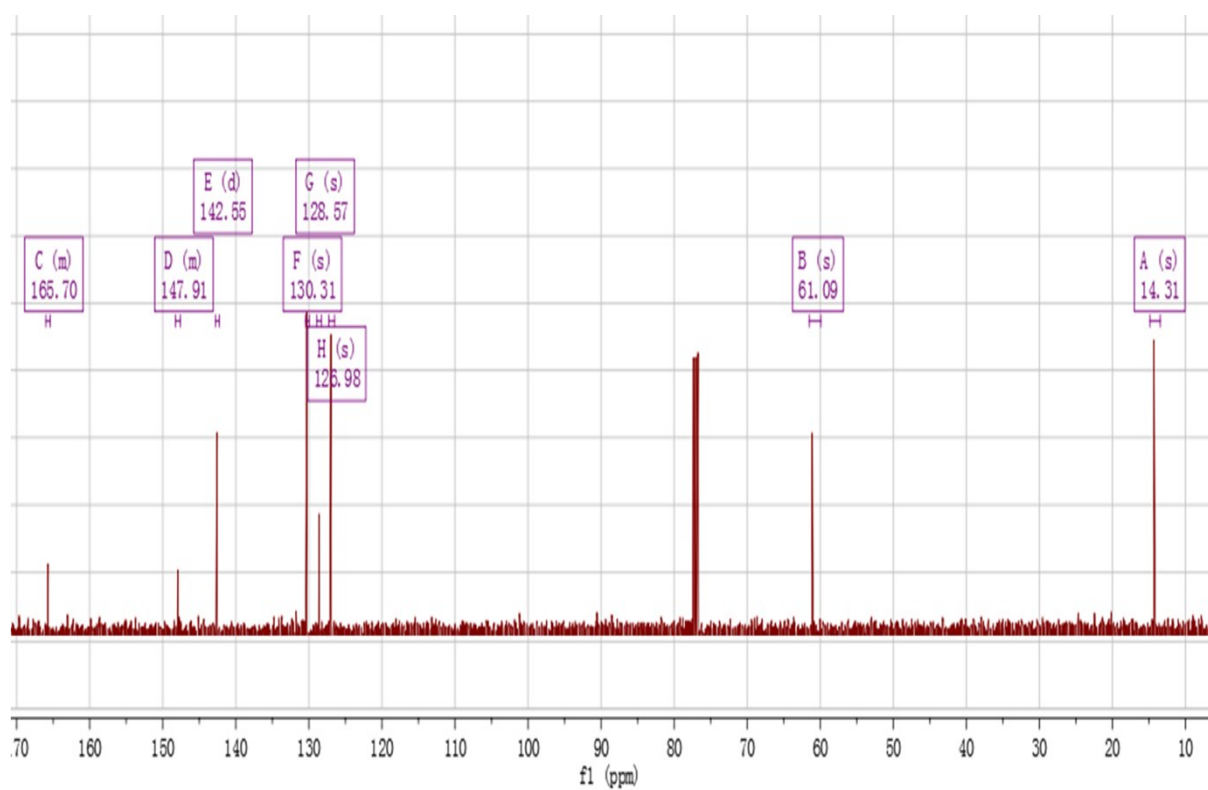
¹³C NMR spectra (400 MHz, DMSO-d₈, 298 K) of **2**



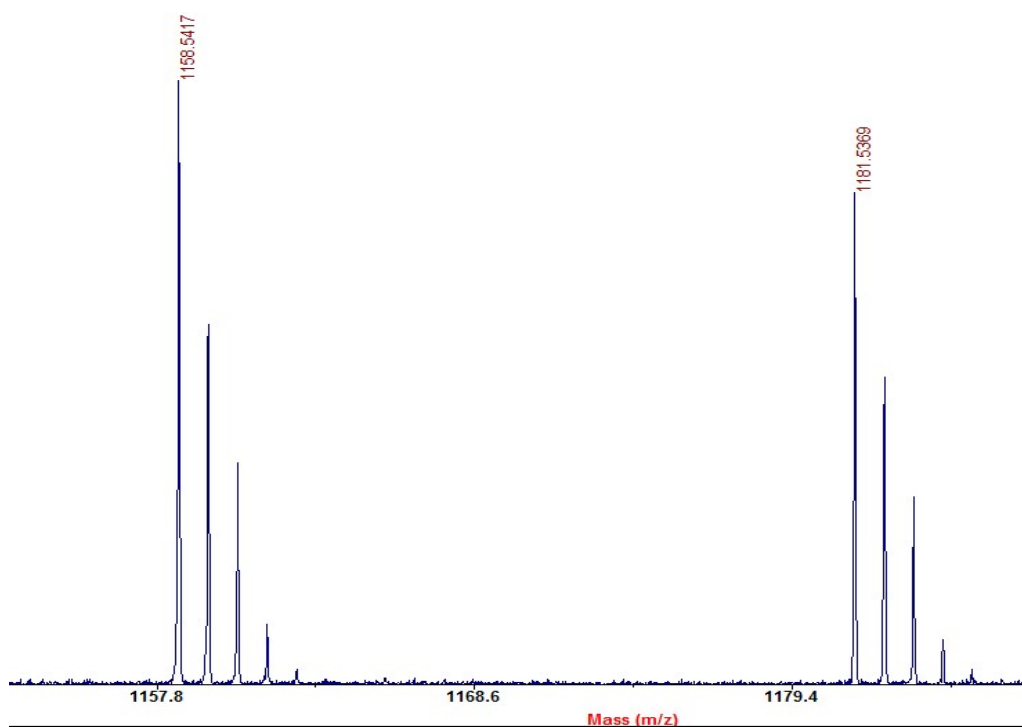
MALDI-TOF MS full spectrum of **2**



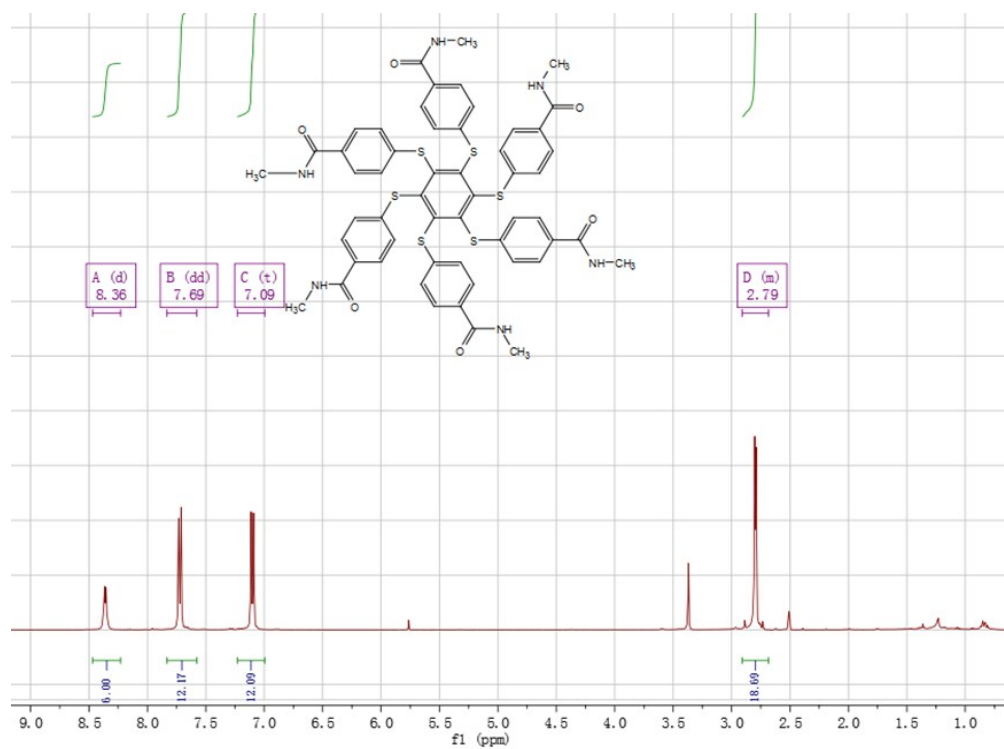
^1H NMR spectra (400 MHz, DMSO- d_6 , 298 K) of **3-1**



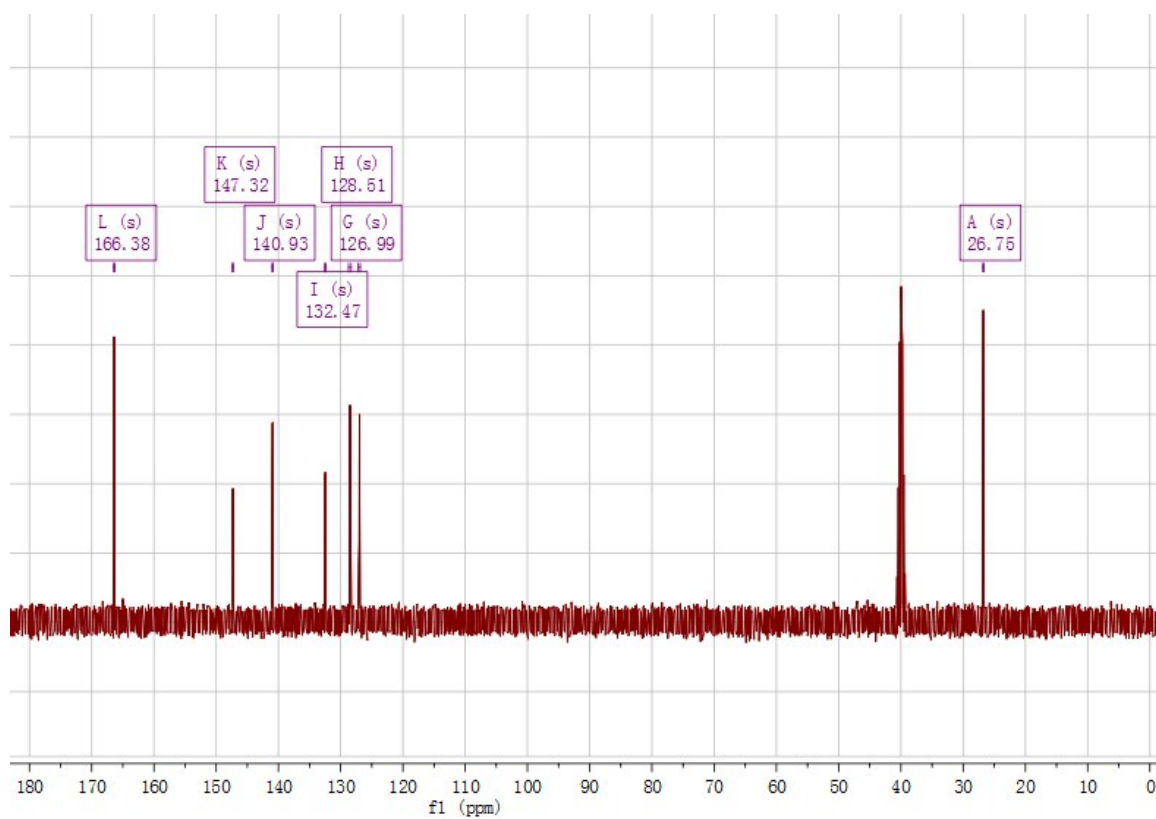
^{13}C NMR spectra (400 MHz, DMSO- d_6 , 298 K) of **3-1**



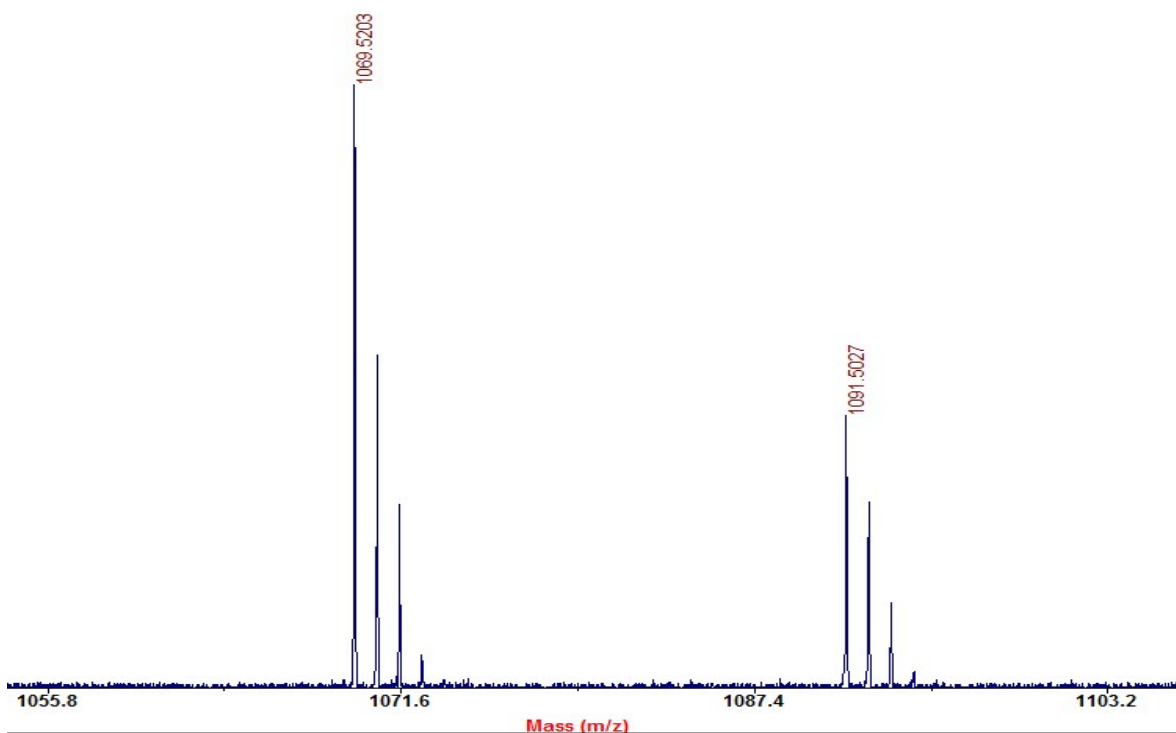
MALDI-TOF MS full spectrum of **3-1**



^1H NMR spectra (400 MHz, DMSO-d_8 , 298 K) of **3**



^{13}C NMR spectra (400 MHz, DMSO-d_6 , 298 K) of **3**



MALDI-TOF MS full spectrum of

Section S17 Reference

Reference

- [S1] F. Saeed and J. Kosar, *Chinese Journal of Catalysis*. 2014, **35**, 368.
- [S2] D. A. Becke, *J. Chem. Phys.* 1993, **98**, 5648.
- [S3] W. J. Hehre, R. Ditchfield, *J.A. J. Chem. Phys.* 1972, **56**, 2257.
- [S4] C. I. Bayly, P. Cieplak, W. Cornell, P.A. Kollman, *J. Phys. Chem.* 1992, **97**, 10269.
- [S5] J. Wang, R. M. Wolf, J. W. Caldwell, P. A. Kollman, D. A. Case, *J. Comput. Chem.* 2004, **25**, 1157.
- [S6] B. Hess, C. Kutzner, D. Van der Spoel, E. Lindahl, *J. Chem. Theory Comput.* 2008, **4**, 435.